Theoretical investigation of $X_{12}O_{12}$ (X = Be, Mg, and Ca) in sensing CH_2N_2 A DFT study

Mohammadi, Mohsen Doust; Abdullah, Hewa Y.; Bhowmick, Somnath; Biskos, George

DOI
10.1016/j.comptc.2021.113168

Publication date
2021

Document Version
Accepted author manuscript

Published in
Computational and Theoretical Chemistry

Theoretical investigation of $X_{12}O_{12}$ (X=Be, Mg, and Ca) in sensing CH_2N_2: A DFT study

Mohsen Doust Mohammadi,[a] Hewa Y. Abdullah[b,*], Somnath Bhowmick,[c] George Biskos,[c,d]

[a] *School of Chemistry, College of Science, University of Tehran, Tehran 14176, Iran*

[b]*Physics Education Department, Faculty of Education, Tishk International University, 44001, Erbil, Iraq*

[c]*Climate & Atmosphere Research Centre, The Cyprus Institute, 20 K. Kavafi Street, Nicosia 2121, Cyprus*

[d]*Faculty of Civil Engineering and Geosciences, Delft University of Technology, Delft 2628 CN, The Netherlands*

***corresponding author** Email: hewayaseen@gmail.com

Abstract

The feasibility of detecting diazomethane (CH_2N_2) in the gas phase by adsorption onto the exterior surface of inorganic-based $X_{12}O_{12}$ (where X can be Be, Mg, or Ca) nanocages is investigated here using density functional theory (DFT). All the structures, including those of the pristine CH_2N_2 and of the nanocages, as well as of the CH_2N_2/nanocage systems, have been optimized using the B3LYP-D3, M06-2X, ωB97XD, and CAM-B3LYP functionals, in conjunction with 6-311G(d) basis set. Natural Bond Orbital (NBO), Non-Covalent Interaction (NCI), and Quantum Theory of Atoms In Molecules (QTAIM) analyses results are in good agreement with each other. Furthermore, the Density Of States (DOSs), the natural charges, the Wiberg Bond Indices (WBI), and natural electron configurations were considered to investigate the nature of intermolecular interactions. The energy calculations indicate a strong size-dependent adsorption, with the nanocages comprised of large atoms being able to attract CH_2N_2 more strongly, and hence bind with it more effectively. The adsorption incurs also significant changes to the Highest Occupied Molecular Orbital (HOMO) and Lowest Unoccupied Molecular Orbital (LUMO) energies.

Keyword: DFT; Diazomethane; Nanocage; NBO; QTAIM.

1. Introduction

Diazomethane (CH_2N_2) is a commonly used methylating agent that is a strong respiratory irritant, posing significant health concerns. At room temperature it is an extremely explosive gas, and thus comprises an important safety hazard [1]. As a result, there is an increasing demand in designing and developing sensors that can measure the concentration of diazomethane in the air for safety reasons.

Among the various types of sensors, those relying on the adsorption of the target gas (i.e., diazomethane in our case) on the sensing material, which consequently alter one measurable property (e.g., their resistance [2]. are very promising for a number of reasons including their simplicity and low fabrication cost. Design such sensing materials, however, requires good understanding of the interaction (i.e., adsorption) between the target gas and the sensing element, which in turns warrants for systematic theoretical calculations.

Density functional theory (DFT), due to its high computational effectiveness for large molecules and its considerable accuracy, provides a suitable framework for theoretical studies of various chemical systems [3]. As a result, it is widely employed to understand the properties of chemical structures and material systems. At the same time, theoretical studies on nanoscaled structures have become well-established in computational chemistry, providing numerous computational tools to study intermolecular interactions and to design materials that can exhibit enhanced performance for specific applications [4-11]. For instance, a wide range of nanomaterials have been developed and tested for gas sensors that can have low limits of detection, high measurement accuracy, low response time, resistant to variable environmental conditions, as well as low production cost [12-18].

Since the discovery of the C_{60} fullerene (which can be considered as the first synthesized nanocage) by Kroto *et al*. [19], numerous studies have investigated its unique properties, which distinguish it as a new carbon allotrope, in view of specific applications. Several experimental and theoretical studies carried out over the past decade have extended this activity by developing and studying structures similar to those of fullerenes, using elements from the third through the fifth groups of the periodic table [20-22]. Following this development, a significant number of studies have investigated the properties of these nanostructures for potential applications in medicine [23], optics [24], quantum computing [25], and electronics [26].

X_nY_n (where X can be B, Al, or Ga, and Y can be N, P, or As) nanocages have a number of unique properties that can be useful for specific gas sensors. For instance, boron nitride (B_nN_n) nanocages are isoelectronic, which is in contrast to carbon fullerene-like nanocages, and exhibit unique optical, magnetic, and electronic properties. In this regard, the Coulomb blockade, photoluminescence and super magnetism of B_nN_n nanocages are significantly disparate compared to those of fullerenes [27]. Earlier theoretical investigations using DFT show the feasibility of adsorption of specific gaseous molecules, including formaldehyde [22], ammonia [28], CO [29], CO_2 [30], NO, N_2O [31], H_2, N_2 and CH_4 [32], *etc*., on $B_{12}N_{12}$ nanocages. Similar theoretical studies, but using other nanocages, including $Ga_{12}N_{12}$ [33], $B_{12}P_{12}$ [21], $Al_{12}P_{12}$ [21], $Ga_{12}P_{12}$ [34], $B_{12}As_{12}$ [35], $Al_{12}As_{12}$ [36], $Ga_{12}As_{12}$ [37], have also been reported.

Earlier studies have shown that $X_{12}O_{12}$ (X = Be, Mg, and Ca) nanocages can act as very effective adsorbents due to the highly ionic metal-oxide bond [38]. For example, Farrokhpour *et*

al. have demonstrated that sulphur mustard can effectively adsorb on $Mg_{12}O_{12}$ nanocages [39], whereas Solimannejad *et al.* have theoretically shown that diazomethane can be adsorbed on silicon carbide nanotubes [40]. Here we report a systematic study on the adsorption of diazomethane molecule onto all six available adsorption sites of $X_{12}O_{12}$ (X = Be, Mg, and Ca) fullerene-like nanocages. The electronic properties, energetic parameters, and geometry optimization of all structures were investigated using Natural Bond Orbital (NBO), Non-Covalent Interaction (NCI), and Quantum Theory of Atoms In Molecules (QTAIM) analysis. All the geometry optimization calculations have been carried out by DFT using four different functionals (i.e., B3LYP-D3, M06-2X, ωB97XD, and CAM-B3LYP), together with a split-valence triple-zeta (6-311G(d)) basis set. The nature of the intermolecular interactions between the gas molecule and the above-mentioned nanocages were studied.

2. Computational details

All the structures investigated in this work have been optimized (assuming vacuum conditions) using the Kohn-Sham DFT [41-42]. Various functionals including CAM-B3LYP [43], M06-2X [44], ωB97XD [45], and the B3LYP-D3 scheme of Grimme [46], together with split-valence triple-zeta basis sets with d-type Cartesian-Gaussian polarization functions (6-311G(d)) were employed. It should be noted that the 6-311G(d) basis set is suitable for the systems considered in this work, as reported in a benchmark study by Grimme *et al*. [47]. No symmetry constraints were imposed. All the molecular geometries were built using the GaussView 6.0.16 [48] software package, which is fully optimized according to the Berny [49] method in Gaussian 16 Rev. C.01 [50] Linux based version of the software. The optimization processes were performed using the default Gaussian convergence criteria. A frequency calculation has been performed to ascertain the stability of each structure and to determine the nature of each stationary point. In addition, wave function stability calculations have also been used to evaluate the stability of the electrons. NBO calculations were carried out using the NBO v 3.1 software (which is integrated within the Gaussian package) to determine the charge-transfer interactions between occupied and unoccupied orbitals. To extract the result data of NBO, NCI, and QTAIM analysis, as well as to depict the DOS diagrams, we employed respectively the Multiwfn [51] and the GaussSum [52] software.

The energy of adsorption (E_{ads}) between two fragments (i.e., the nanocage and the CH_2N_2 gas molecule) can be considered as follows:

$$E_{ads} = E_{cage/gas} - E_{cage} - E_{gas} + \Delta E_{(BSSE)} \quad (1)$$

where $E_{cage/gas}$ is the total energy of the gas/nanocage cluster, E_{cage} and E_{gas} are the energies of the isolated nanocage and isolated gas molecule, respectively, and $\Delta E_{(BSSE)}$ is the Basis Set Superposition Error (BSSE) obtained from the Boys and Bernardi's counterpoise procedure [51] as follows:

$$\Delta E_{(BSSE)} = \Delta E_{cluster} - \Delta E_{cage}^{cluster} - \Delta E_{gas}^{cluster} \quad (2)$$

According to Equation 1, negative values of E_{ads} (i.e., corresponding to exothermic adsorptions) indicate that the formed complex is stable; otherwise, positive values of E_{ads} belong to a local

minimum in which the adsorption of CH_2N_2 on the surface of the nanocage is deterred by an energy barrier.

3. Results and discussion

3.1 Structural analysis

The structures of pristine $X_{12}O_{12}$ nanocages were optimized using DFT at the CAM-B3LYP/6-311G(d) level. Although CAM-B3LYP describes the long-range interactions, it does not consider dispersion correction and the charge transfer excitations; therefore, all of the structures were re-optimized using robust methods (i.e., M06-2X, ωB97XD, and B3LYP-D3). Head-Gordon *et al*. [45] developed the ωB97XD functional to account to capture the effect of long-range interactions and to make dispersion-related corrections. Among the functionals of the Minnesota 06 suit, developed by Truhlar *et al*. [44], the global hybrid functional with double non-local exchange (2X) amounts (i.e., M06-2X) is a high-performance method to study the non-covalent interactions. To take into account the effect of dispersion, the latest version of B3LYP-D3, known as D3 (BD) (GD3BJ) developed by Grimme *et al*. [46], would also be a good option and has been used in this present study.

The geometrical structure of the $X_{12}Y_{12}$ nanocages containing the X-Y bonds is shown in Figure 1. These nanocages consist of eight (8) symmetric hexagons and six (6) tetragons having an equal number of adsorption positions for the adsorption of any molecule onto their outer surface shown further below. The adsorption sites can be categorized as follows: on top of the X atom (T_1), on top of the Y atom (T_2), on top of the XY66 bond (T_3), on top of the H-6 position (T_4), on top of the XY64 bond (T_5), and on top of H-4 position (T_6). After the optimization of the pristine nanocage structures, we placed the CH_2N_2 at a vertical distance of approximately 2.5 Å onto the outer surface of the nanocages in any of the six possible adsorption sites.

The optimized geometrical parameters of the CH_2N_2 molecule obtained by all four functionals are in good agreement with experimental results (see Figure S1 in the supplemental material). Evidently, the B3LYP-D3 method gives the best results among all four functionals compared to the observed fundamental vibrational frequencies (see Table S1 in the supplemental material). For example, the B3LYP-D3 C-H stretching frequency was calculated to be 3179 cm^{-1}, which is in good agreement with the experimental value of 3073 cm^{-1}. The optimized structural parameters of the isolated CH_2N_2 gas molecule obtained by the B3LYP-D3 method is depicted in Figure 2.

The optimized structures of the bare $X_{12}O_{12}$ nanocages calculated by the functionals considered in this study are provided in the supplementary material. All four methods have good correspondence with the previous B3LYP/6-31+G(d) calculations by Omidi *et al.* [38]. For example, the X-O bond lengths calculated in this study lies between 1.58-1.61 Å when X is Be, 1.93-1.95 Å when X is Mg and 2.18-2.19 Å when X is Ca, having good agreement with the values obtained by obtained by Omidi *et al.*: i.e., 1.58 Å when X is Be, 1.95 Å when X is Mg and 2.28 Å when X is Ca. The final B3LYP-D3 optimized structures of the pristine nanocages together with

the gas/cage complexes and the corresponding bond lengths are illustrated in Figures 3 and 4 and the corresponding atomic co-ordinates are provided in the supplementary material.

It should be stressed that to find the optimum distance between the nanocage and the adsorbed gas molecule, we used rigid scans in the PM7/6-311G(d) level of theory. The logical approach is to place the gas molecule in each of these positions and calculate the amount of adsorption energy (E_{ads}). Our experience shows that negligible differences exist in the amounts of adsorption energies when we place the gas in any of the six possible adsorption sites. As mentioned by Foresman *et al.* [54], when the differences in the adsorption energies are "below the range of chemical interest", placing the gas molecule in different positions on the nanocages provides identical results. Next, regarding the amount of E_{ads} values, some structures were chosen for DFT calculations at CAM-B3LYP/6-311G(d) level of theory. Finally, structures with the most negative energy were selected for the re-optimization process using the M06-2X, ωB97XD, and B3LYP-D3 functional and the 6-311G(d) basis set. The B3LYP-D3 functional is the basis for decision making to study interactions that consider dispersion corrections and are in good agreement with the experimental observations, whereas the rest of the functionals are given here for comparison only. The E_{ads} values obtained from optimization calculations are provides in Tables 1 and 2.

The adsorption energies (E_{ads}) calculated by the B3LYP-D3 method at all six adsorption sites are reported in Table 1. As discussed previously, the choice of the adsorption site has a negligible effect on the corresponding adsorption energies, although the XY64 site releases the largest energy compared to others. The maximum difference in E_{ads} among all adsorption sites is found to be around 0.03 eV. Table 2 provides the calculated E_{ads} on the $X_{12}O_{12}$ nanocages at the XY64 site obtained using different functionals. From these values, it is clear that as the size of the atoms in the nanocages decreases, the intensity of adsorption between the gas molecule and the nanocages increases. For example, in the case of CAM-B3LYP/6-311G(d) optimization of $CH_2N_2/Be_{12}O_{12}$, $CH_2N_2/Mg_{12}O_{12}$, and $CH_2N_2/Ca_{12}O_{12}$, the adsorption energies are -0.605, -0.546, and -0.446 eV, respectively. It should be noted here that the B3LYP-D3 adsorption energy for diazomethane obtained in this work (-0.71 eV to -0.79 eV) is comparable to the adsorption of sulfur mustard on $Be_{12}O_{12}$ and $Mg_{12}O_{12}$ nanocages (-0.47 eV to -0.99 eV) [39]. This is despite the fact that here we used a triple zeta basis set, in contrast to a double zeta basis that has been employed for the sulfur mustard adsorption study.

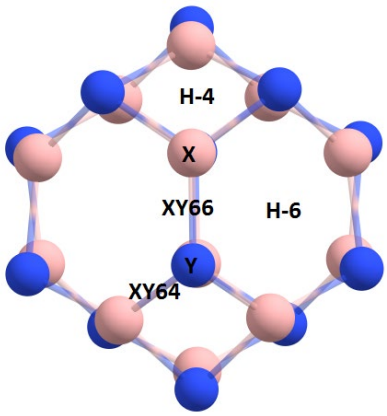

Figure 1. The structure of the $X_{12}Y_{12}$ (where X is Be, Mg, or Ca and Y is O) nanocages, displaying all adsorption sites, including the X-site (on top of the X atom), Y-site (on top of the Y atom), H-6 site (on top of the hexagonal ring), H-4 site (on top of the tetragonal ring), XY66 site (on top of the atomic bond between two hexagonal rings) and XY64 site (on top of the atomic bond between tetragonal and hexagonal rings).

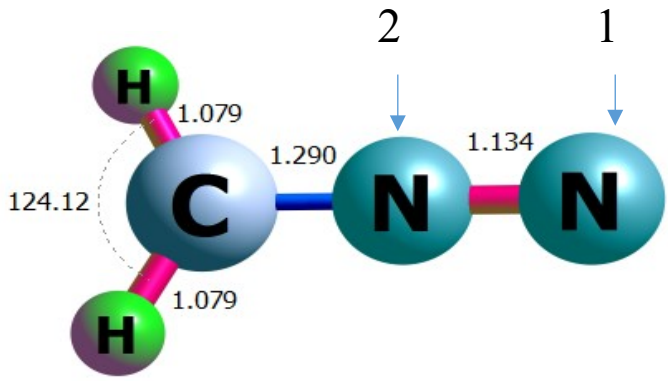

Figure 4. Optimized structure of CH_2N_2 gas molecule obtained from B3LYP-D3/6-311G(d) level of theory. The unit of the bond lengths are given in Å and the angles in degrees.

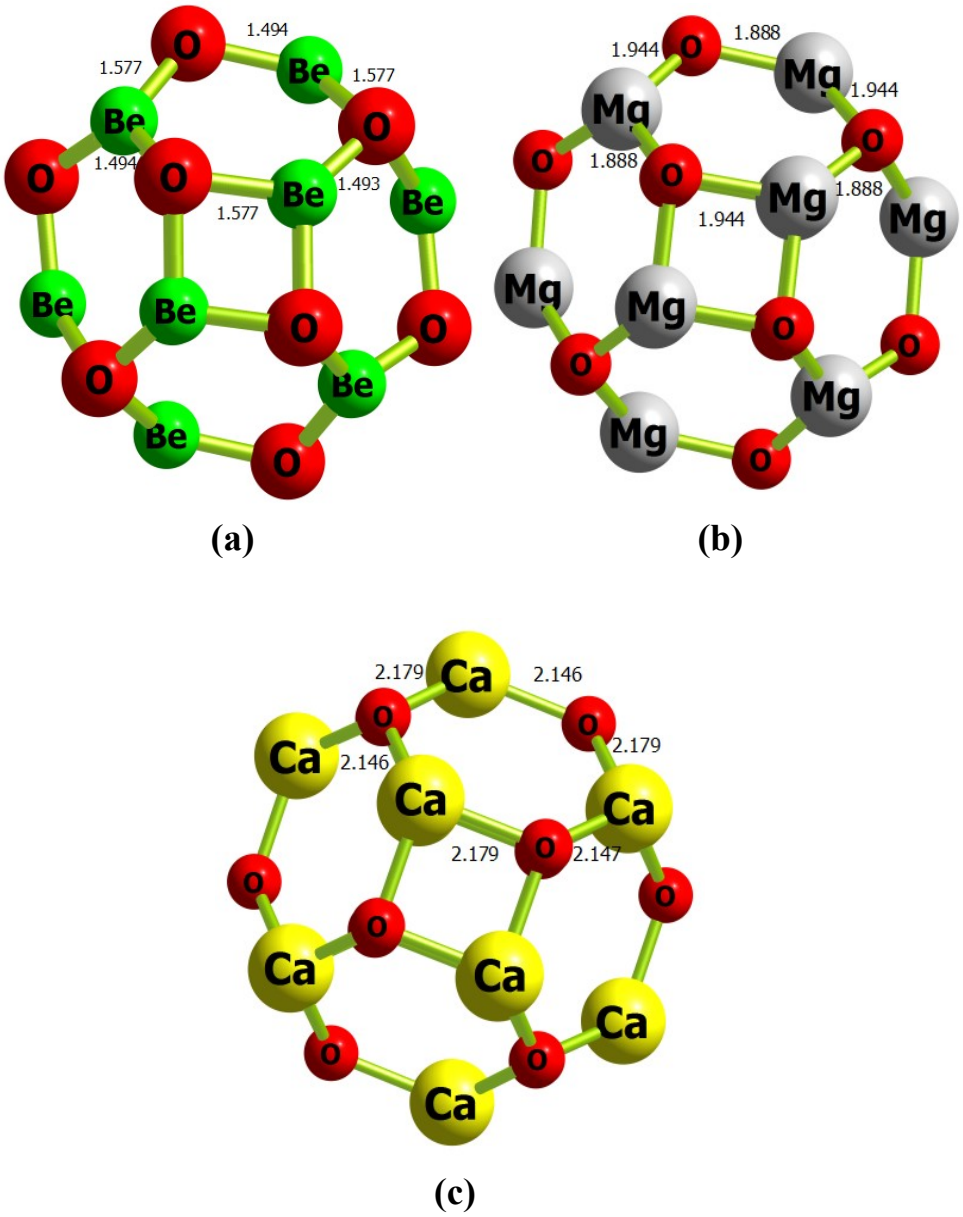

Figure 3. The bond length (Å) obtained at B3LYP-D3/6-311G(d) level for **(a)** $Be_{12}O_{12}$, **(b)** $Mg_{12}O_{12}$, and **(c)** $Ca_{12}O_{12}$.

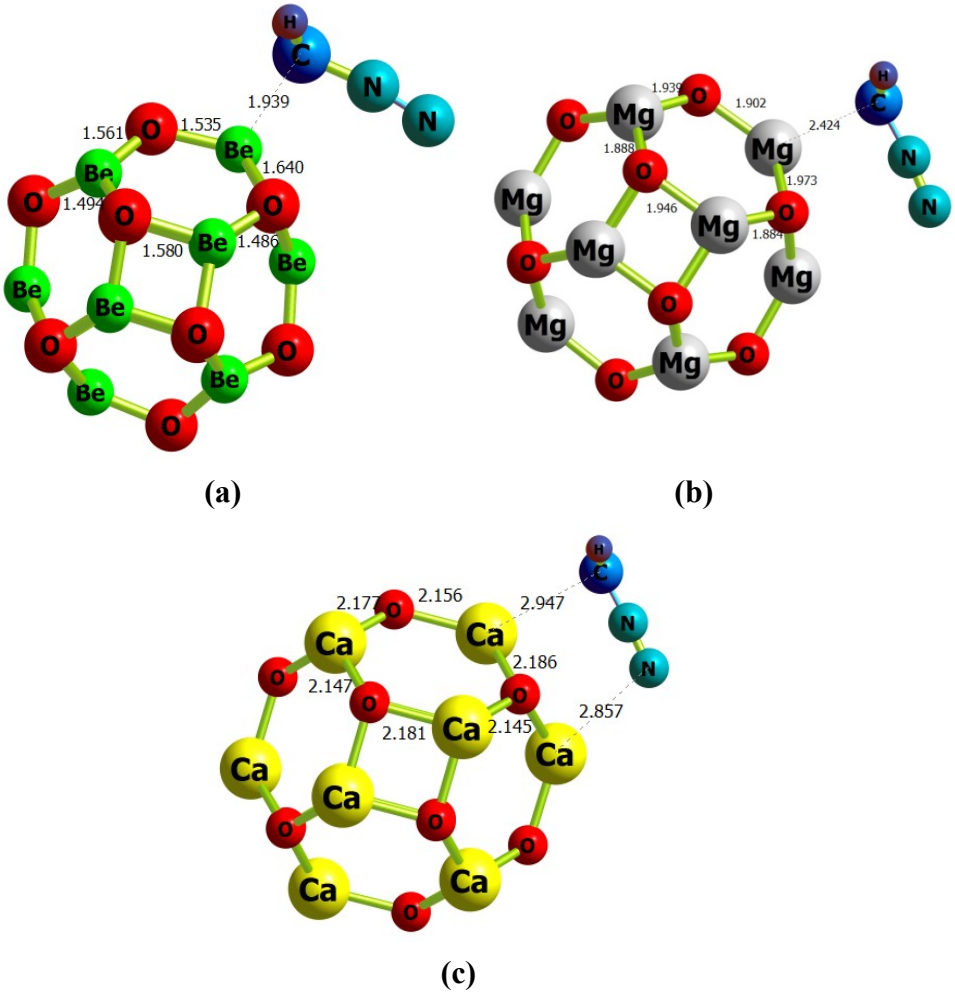

Figure 4. The optimized structures of **(a)** $CH_2N_2/Be_{12}O_{12}$, **(b)** $CH_2N_2/Mg_{12}O_{12}$, and **(c)** $CH_2N_2/Ca_{12}O_{12}$ obtained from B3LYP-D3/6-311G(d) level of theory. The units of the bond lengths are given in Å.

Table 1

Adsorption energies (E_{ads}) for $CH_2N_2/X_{12}O_{12}$ (where X is Be, Mg, or Ca) complexes calculated at X, Y, H-4, H-6, XY64 and XY66 adsorption sites. All values are expressed in eV and are obtained from geometry optimization calculations using the B3LYP-D3 functional in combination with 6-311G(d) basis set.

System	X	Y	H-4	H-6	XY64	XY66
$CH_2N_2/Be_{12}O_{12}$	0.012	0.014	0.002	0.030	0.0	0.014
$CH_2N_2/Mg_{12}O_{12}$	0.009	0.001	0.002	0.004	0.0	0.012
$CH_2N_2/Ca_{12}O_{12}$	0.005	0.015	0.003	0.001	0.0	0.008

Table 2

Adsorption energies (E_{ads}) for $CH_2N_2/X_{12}O_{12}$ (wher X is Be, Mg, or Ca) complexes at the XY64 adsorption site. All values are expressed in eV and are obtained from geometry optimization calculations using the CAM-B3LYP, M06-2X, ωB97XD, and B3LYP-D3 functionals in combination with 6-311G(d) basis set.

Systems	B3LYP-D3	CAM-B3LYP	M06-2X	ωB97XD
$CH_2N_2/Be_{12}O_{12}$	-0.712	-0.605	-0.804	-0.676
$CH_2N_2/Mg_{12}O_{12}$	-0.743	-0.546	-0.748	-0.633
$CH_2N_2/Ca_{12}O_{12}$	-0.699	-0.446	-0.610	-0.521

2.1 Electronic Structure

The "Conceptual DFT" has been developed to consider the reactivity concept. Various properties can be obtained from the HOMO-LUMO energy gap (HLG) [55]. For example, when an external potential applied to a system, within the Hohenberg-Kohn context [41,42], the HOMO and LUMO energies are related to the ionization potential (IP) and electron affinity (EA). One can also easily show that the electronegativity (χ) is equal to the negative chemical potential (μ). Furthermore, the electrophilicity index (ω) is inversely related to the chemical hardness (η), which in turn is related to the difference between IP and EA. The calculated values of these properties are listed in Table 3.

The HOMO-LUMO energy gap (ΔE_g) of $Be_{12}O_{12}$, $Mg_{12}O_{12}$, and $Ca_{12}O_{12}$ have been calculated to be 8.43, 4.86, and 3.56 eV, respectively, at the B3LYP-D3/6-311G(d) theory level. The adsorption of CH_2N_2 on its surface will reduce the energy gap to 5.33, 4.20, and 2.60 eV, respectively. These results show the sensitivity of the HOMO-LUMO energies with respect to adsorption. From the results provided in Table 3, it is also evident that the LUMO values were largely stabilized compared to the destabilization of the HOMO orbitals.

The sensor response (S) is defined as $S = exp\left(\frac{|\Delta E_g|}{kT}\right) - 1$, where k is the Boltzmann constant and T the temperature expressed in Kelvin. It is clear that the resistivity diminishes when the energy gap ΔE_g is reduced since the resistivity is proportional to the reciprocal of the conducting electron population. Hence, the resistivity of the tube upon adsorption of gas molecules is low, and the electric current generated in the circuit will exhibit the lowest resistance. The density of state (DOS) map is useful for intuitively revealing the density of distribution of the molecular orbitals in different energy regions, and the gap is directly visible from this map (see Figure 5).

Table 3

HOMO energy (ε_H), LUMO energy (ε_L), Fermi energy (E_F), HOMO–LUMO energy gap (HLG), chemical potential (μ), chemical hardness (η), and electrophilicity (ω) of the pristine $X_{12}O_{12}$ nanocages and the $CH_2N_2/X_{12}O_{12}$ complexes (where X is Be, Mg, or Ca). All values are in eV and were obtained using the B3LYP-D3/6-311G(d) level of theory.

Systems	ε_H	ε_L	E_F	HLG	μ	η	ω
$Be_{12}O_{12}$	-8.672	-0.237	-4.455	8.435	-4.455	4.218	41.848
$Mg_{12}O_{12}$	-6.543	-1.680	-4.111	4.864	-4.111	2.432	20.553
$Ca_{12}O_{12}$	-4.649	-1.089	-2.869	3.560	-2.869	1.780	7.324
$CH_2N_2/Be_{12}O_{12}$	-7.723	-2.393	-5.058	5.330	-5.058	2.665	34.090
$CH_2N_2/Mg_{12}O_{12}$	-6.287	-2.091	-4.189	4.196	-4.189	2.098	18.406
$CH_2N_2/Ca_{12}O_{12}$	-4.527	-1.931	-3.229	2.596	-3.229	1.298	6.766

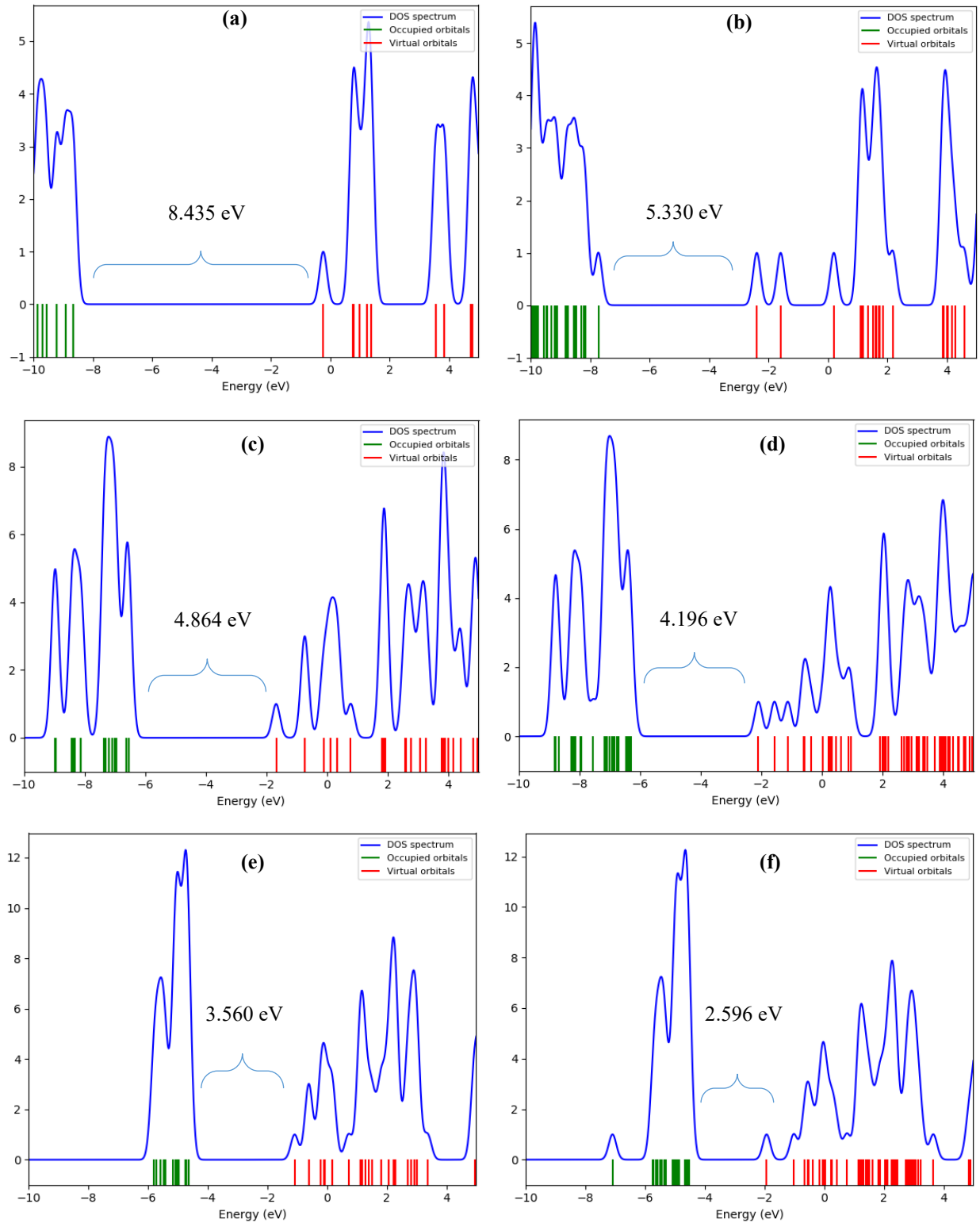

Figure 5. Density of state maps for **(a)** $Be_{12}O_{12}$, **(b)** $CH_2N_2/Be_{12}O_{12}$, **(c)** $Mg_{12}O_{12}$, **(d)** $CH_2N_2/Mg_{12}O_{12}$, **(e)** $Ca_{12}O_{12}$, and **(f)** $CH_2N_2/Ca_{12}O_{12}$. Data were obtained from the B3LYP-D3/6-311G(d) level of theory.

2.2 Natural Bond Orbital (NBO) Analysis

The NBO method, developed by Weinhold *et al*. [56], is one of the most robust population analysis methods that can determine the electron density distribution within bonds between the atoms. The term NBO refers to a bonding orbital with the maximum electron density. A density matrix, calculated from the DFT method, and the atomic charge, is used to define the natural bonding orbitals. In order to complete the span of the valance space, in addition to the bonding NBOs (σ), determination of antibonding NBOs (σ*) is also required. In the present study, the NBO calculations have been performed to evaluate various types of bond order, including Mulliken [57] and Mayer [58] bond order as well as Wiberg bond index (WBI) in Löwdin orthogonalized basis [59]. Mulliken and Mayer's bond orders are sensitive to the chosen basis set, especially for the basis set that includes diffuse functions. On the other hand, the Wiberg bond order is less dependent on the basis set in comparison to the other two. Additionally, the Fuzzy Bond Order (FBO) was proposed by Mayer [60], and the Laplacian bond order proposed by Lu [61] has also been calculated from the corresponding overlap and density matrix. In Table 4, we report the calculated C-X bond orders based on these different methods. Evidently, there is a correlation between the size of the cation in the nanocages and the bond order: *i.e*., the larger the cation, the lower the bond order. The bond order values also signify that the interaction of the gas with the nanocages can be classified as strong interactions.

We have also calculated the natural charges and natural electron configuration data through natural population analysis combined with NBO (cf. Table 5). Using the NBO analysis, the nature of the intermolecular interaction between the gas molecule and nanocages becomes more intelligible. As reflected by the calculates reported in Table 5, the existence of charge transfer within these complexes is very obvious. The valance shell of each atom in CH_2N_2 is changed due to the interaction with the nanocages. For example, the valence shell of C atom in molecules of the gas phase is 2*s*(1.03) 2*p*(3.43) 3*p*(0.01), which is changed to 2*s*(1.17) 2*p*(3.53) 3*s*(0.01) 3*p*(0.02) for the $Be_{12}O_{12}$/gas complex during the adsorption process. This result suggests that a strong interaction has occurred.

Table 4
Values of Mulliken, Mayer, and Wiberg, Fuzzy, and Laplacian bond orders obtained for the interactions of the CH_2N_2 molecule and $X_{12}O_{12}$ (where X is Be, Mg, or Ca). All calculations were performed using the B3LYP-D3/6-311G(d) theory level.

System	$X^a....Y^b$	Mulliken	Mayer	FBO	WBI	Laplacian
$CH_2N_2/Be_{12}O_{12}$	C.....Be	0.204	0.259	0.449	0.528	0.112
$CH_2N_2/Mg_{12}O_{12}$	C.....Mg	0.203	0.214	0.442	0.391	0.084
$CH_2N_2/Ca_{12}O_{12}$	C.....Ca	0.099	0.128	0.252	0.180	0.069

(a) X atoms are belong to CH_2N_2
(b) Y atoms are belong to Nanocages

Table 5
Natural charge (in *a.u.*) and natural electron configurations for the CH_2N_2 and $CH_2N_2/X_{12}O_{12}$ structures (where X is Be, Mg, or Ca). All values have been obtained from NBO analysis using the B3LYP-D3/6-311G(d) level of theory.

Systems	atom	Natural Charge	Natural Electron Configuration
CH_2N_2	C	-0.480	[core] 2*s*(1.03) 2*p*(3.43) 3*p*(0.01)
	H1	0.243	1*s*(0.76)
	H2	0.243	1*s*(0.76)
	N1	0.021	[core] 2*s*(1.14) 2*p*(3.81) 3*s*(0.01) 3*p*(0.02) 3*d*(0.01)
	N2	-0.026	[core] 2*s*(1.61) 2*p*(3.39) 3*s*(0.01) 3*p*(0.01) 3*d*(0.01)
$CH_2N_2/Be_{12}O_{12}$	C	-0.728	[core] 2*s*(1.17) 2*p*(3.53) 3*s*(0.01) 3*p*(0.02)
	H1	0.279	1*s*(0.72)
	H2	0.279	1*s*(0.72)
	N1	0.107	[core] 2*s*(1.16) 2*p*(3.71) 3*s*(0.01) 3*p*(0.02)
	N2	0.117	[core] 2*s*(1.60) 2*p*(3.25) 3*s*(0.01) 3*p*(0.01) 3*d*(0.02)
$CH_2N_2/Mg_{12}O_{12}$	C	-0.661	[core] 2*s*(1.12) 2*p*(3.50) 3*s*(0.01) 3*p*(0.02)
	H1	0.271	1*s*(0.73)
	H2	0.271	1*s*(0.73)
	N1	0.089	[core] 2*s*(1.15) 2*p*(3.73) 3*s*(0.01) 3*p*(0.02) 3*d*(0.01)
	N2	0.064	[core] 2*s*(1.60) 2*p*(3.31) 3*s*(0.01) 3*p*(0.01) 3*d*(0.01)
$CH_2N_2/Ca_{12}O_{12}$	C	-0.557	[core] 2*s*(1.07) 2*p*(3.46) 3*p*(0.02)
	H1	0.261	1*s*(0.74)
	H2	0.261	1*s*(0.74)
	N1	0.077	[core] 2*s*(1.14) 2*p*(3.75) 3*s*(0.01) 3*p*(0.02) 3*d*(0.01)
	N2	-0.038	[core] 2*s*(1.60) 2*p*(3.41) 3*s*(0.01) 3*p*(0.01) 3*d*(0.01)

2.3 Quantum Theory of Atoms In Molecules (QTAIM) Analysis

QTAIM analysis has been used to study the bond types and intermolecular interactions. A critical point of the electron density, including minimum, maximum, or saddle point, can belong to: (1) *atomic critical point* (ACP); (2) *bond critical point* (BCP); (3) *ring critical point* (RCP); and (4) *cage critical point* (CCP). The electron density $\rho(\mathbf{r})$ and the Laplacian electron density $\nabla^2\rho(\mathbf{r})$ play an essential role in the QTAIM analysis since they determine the segmentation and identification of different types of chemical interactions. A bond critical point with negative values of the Laplacian electron density and large values of the electron density ($\rho(\mathbf{r})>10^{-1}$ *a.u.*) is defined as a covalent bond. On the other hand, the positive value of $\nabla^2\rho(\mathbf{r})$ designates that the interactions

can be classified as of the non-substrate close-shell type (which include ionic and van der Waals interactions) [62].

The values of Lagrangian kinetic energy $G(\mathbf{r})$ and potential energy density $V(\mathbf{r})$ divulges the nature of the intermolecular interaction; therefore, the ratio of $G(\mathbf{r})/|V|(\mathbf{r})$ can be hired as an appropriate index in link classification. When $G(\mathbf{r})/|V|(\mathbf{r}) < 0.5$, the nature of the interaction is covalent, and if $G(\mathbf{r})/|V|(\mathbf{r}) > 1.0$, the interaction is non-covalent. On the other hand, a large value of the elliptical bond (ε) represents an unstable structure and is related to the ratio between the eigenvalues (λ_1, λ_2,.. etc.) of the Hessian matrix [63].

Table 6 provides the calculated values of these parameters obtained from the QTAIM analysis. Since all values for $\nabla^2\rho(\mathbf{r})$ are positive and the $\rho(\mathbf{r})$ values are always less than 0.1, we can safely assume that the stabilities of the adsorbed complexes originate from the non-covalent or van der Waals interactions. Moreover, the $G(\mathbf{r})/|V|(\mathbf{r})$ ratios are higher than unity, except for the C....Be interaction in the $CH_2N_2/Be_{12}O_{12}$ cluster. These results suggest that intermolecular interactions can be classified as non-covalent. The calculated values of the elliptical bonds are also very small, indicating that the structures are highly stable. Figure 6 provides a schematic illustration of the bond critical points between gas and nanocages.

Table 6

QTAIM topological parameters for electron density ρ(r), Laplacian of electron density $\nabla^2\rho$(r), kinetic electron density G(r), potential electron density V(r), eigenvalues of Hessian matrix (λ), and bond ellipticity index (ε) at the BCPs of the CH_2N_2 clusters with $X_{12}O_{12}$ (where X can be Be, Mg, or Ca). All values were calculated using the B3LYP-D3/6-311G(d) level of theory and NBO analysis.

Systems	Bond	ρ	$\nabla^2 r$	G(r)	V(r)	G(r)/$\|V\|$(r)	λ_1	λ_2	λ_3	ε
$CH_2N_2/Be_{12}O_{12}$	C....Be	0.0462	0.2009	0.0561	-0.0621	0.9045	-0.0640	-0.0682	0.3331	0.0671
$CH_2N_2/Mg_{12}O_{12}$	C....Mg	0.0218	0.1029	0.0228	-0.0200	1.1443	-0.0231	-0.0232	0.1492	0.0013
$CH_2N_2/Ca_{12}O_{12}$	C....Ca	0.0130	0.0468	0.0102	-0.0086	1.1791	-0.0101	-0.0109	0.0679	0.0823
	N....Ca	0.0119	0.0484	0.0104	-0.0087	1.1963	-0.0101	-0.0103	0.0688	0.0133

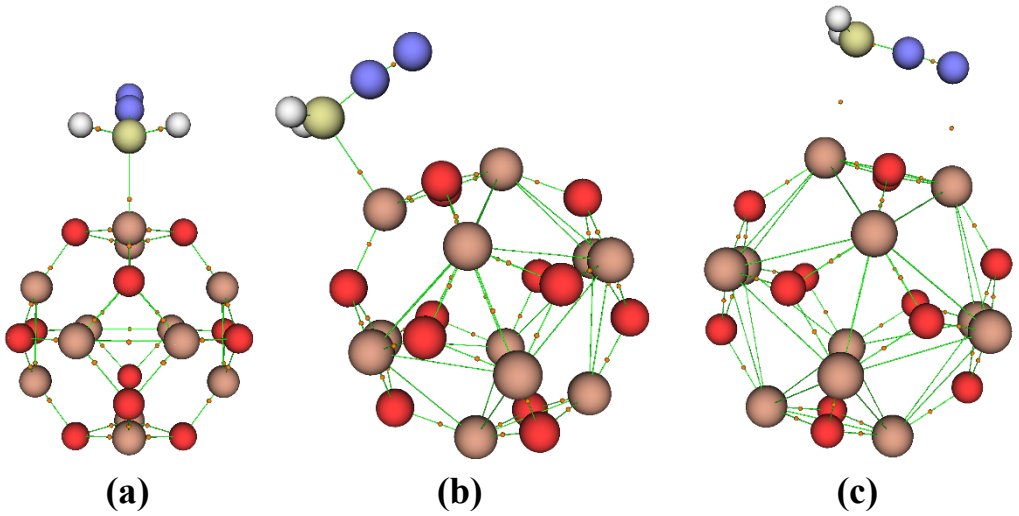

Figure 6. The bond critical points graph for the (a) $CH_2N_2/Be_{12}O_{12}$, (b) $CH_2N_2/Mg_{12}O_{12}$, and (c) $CH_2N_2/Ca_{12}O_{12}$systems. The orange dots represent the BCPs.

The results of QTAIM analysis discussed in the previous section showed that the interactions between CH_2N_2 and nanotubes are essentially non-covalent; hence, it is useful to re-evaluate the interaction with a non-covalent analysis. The reduced density gradient (RDG) and sign$\lambda_2(r)\rho(r)$ are a pair of functions used in non-covalent interaction (NCI) [64] analysis, which can be implemented to visualize the region and the type of weak interactions. Plots of these two functions, RDG and sign$\lambda_2(\mathbf{r})\rho(\mathbf{r})$, can be used to identify specific areas; in particular, the non-covalent interaction area. The points that indicate strong interactions are located in the sign$\lambda_2(\mathbf{r})\rho(\mathbf{r}) < 0$ region. Relatively weak van der Waals interactions are found in the sign$\lambda_2(\mathbf{r})\rho(\mathbf{r}) \approx 0$ region. Furthermore, if points are in sign$\lambda_2(\mathbf{r})\rho(\mathbf{r}) > 0$ region, suggests that the interactions are repulsive [64,65]. As it turns out, bond strength is closely related to the density matrix $\rho(\mathbf{r})$ as well as to signλ_2. Low RDG and low electron density regions should be further consulted to determine whether non-covalent interactions occur between the two components involved in the adsorption process.

From Figure 7, it is evident that non-covalent interaction analysis can adequately describe the interactions between gas and nanocages. In the sign$\lambda_2(\mathbf{r})\rho(\mathbf{r}) < 0$ region, many points are observed, which indicates that there are very strong non-covalent interactions between the two fragments. It is also observed that in the sign$\lambda_2(\mathbf{r})\rho(\mathbf{r}) \approx 0$ region, there is no high concentration of points. Therefore, it can be concluded that the intermolecular interactions during the adsorption process are not van der Waals.

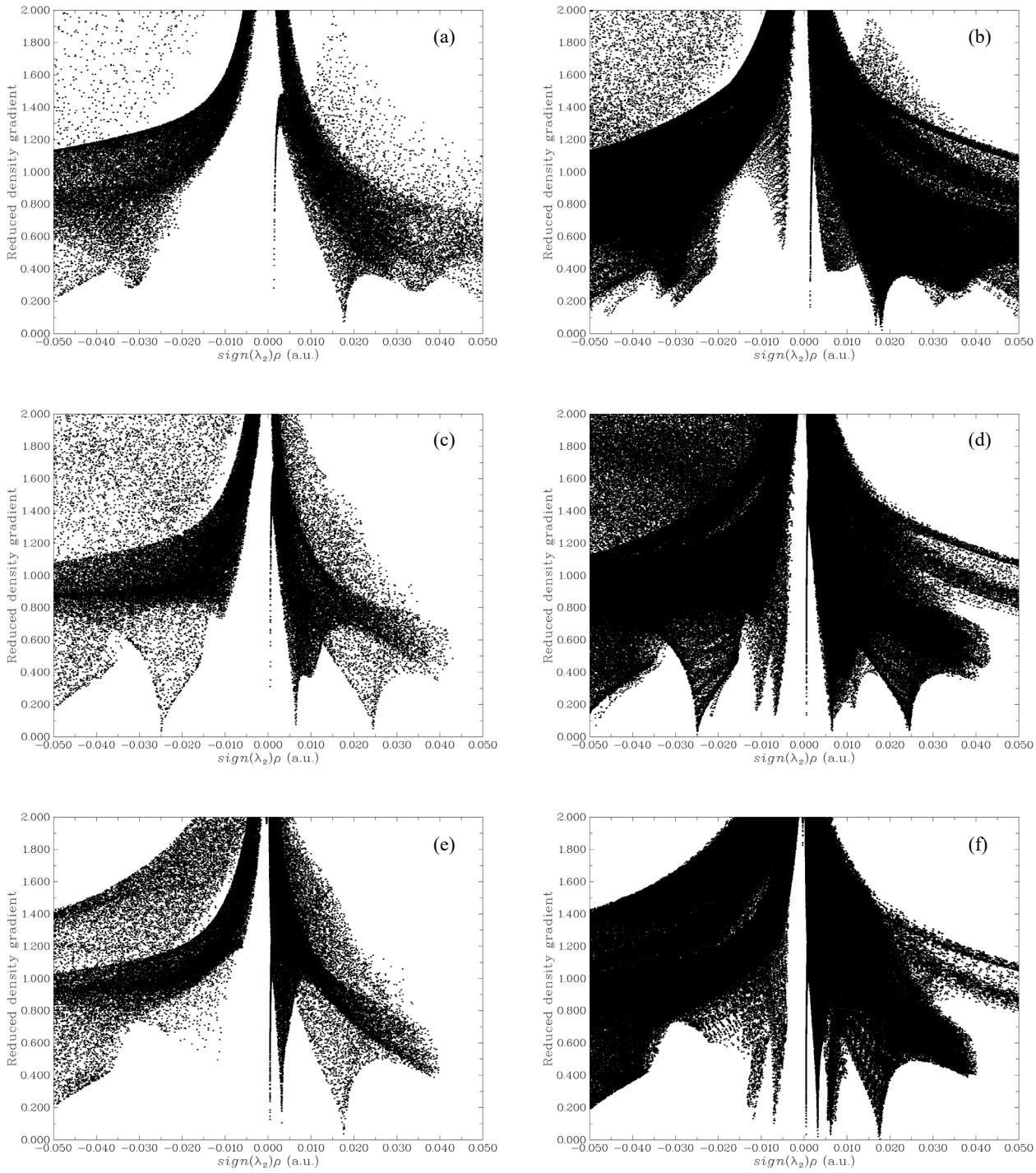

Figure 7. The sign(λ_2)ρ(**r**) (X-axis) vs. RDG (Y-axis) diagrams for **(a)** $Be_{12}O_{12}$, **(b)** $CH_2N_2/Be_{12}O_{12}$, **(c)** $Mg_{12}O_{12}$, **(d)** $CH_2N_2/Mg_{12}O_{12}$, **(e)** $Ca_{12}O_{12}$, and **(f)** $CH_2N_2/Ca_{12}O_{12}$. The diagrams were obtained from B3LYP-D3/6-311G(d) level of theory.

4. Conclusion

The intermolecular interactions between the CH_2N_2 gas molecule and $X_{12}O_{12}$ (where X can be Be, Mg, or Ca) nanocages were studied by DFT. All molecular structures have been optimized using the CAM-B3LYP, M06-2X, ωB97XD, and B3LYP-D3 functionals together with a 6-311G(d) basis set. The optimized structures obtained from B3LYP-D3/6-311G(d) were chosen for population analysis calculations because of their good agreement with earlier experimental and theoretical results. The calculated values of the adsorption energy indicate that on top of the X-O bond connecting the tetragonal and hexagonal rings is the most favourable adsorption site. In general, adsorption energy increases with the size of the central metal atom of the $X_{12}O_{12}$ nanocages. Several bond order analysis data corroborate the above conclusion. To understand the nature of the intermolecular interactions, we further performed NBO, QTAIM, and NCI analyses, with the results appearing to correspond well with each other. The NBO calculations show a significant charge transfer, whereas the NCI and QTAIM results indicate strong intermolecular interactions. To sum up, we conclude that the studied $X_{12}O_{12}$ nanocages have an active surface in favor of the CH_2N_2 gas adsorption. Our findings indicate that nanomaterials containing $X_{12}O_{12}$ nanocages investigated here would be suitable for designing a sensitive CH_2N_2 sensors.

Acknowledgements

HYA thanks the Solid-State Theory Group, Physics Department, Università degli Studi di Milano, Milan, Italy for providing computational facilities. SB and GB acknowledge the support of the European Regional Development Fund and the Republic of Cyprus through the Research Innovation Foundation (Cy-Tera project under the grant NEA YPODOMH/STPATH/0308/31, and NANO^{2}LAB project under the grant INFRASTRUCTURES/1216/0070).

Conflict of Interest

The authors declare no conflict of interest.

References

[1] D. Dallinger, C.O. Kappe, Lab-scale production of anhydrous diazomethane using membrane separation technology, Nature Protocols, 12 (2017) 2138-2147.
[2] N.A. Isaac, M. Valenti, A. Schmidt-Ott, G. Biskos, Characterization of Tungsten Oxide Thin Films Produced by Spark Ablation for NO_2 Gas Sensing, ACS Applied Materials & Interfaces 8 (2016) 3933-3939.
[3] D. Sholl, J.A. Steckel, *Density Functional Theory: A Practical Introduction*, John Wiley & Sons, Inc., Hoboken, New Jersey, 2009.
[4] A.S. Novikov, M.L. Kuznetsov, Theoretical study of Re(IV) and Ru(II) bis-isocyanide complexes and their reactivity in cycloaddition reactions with nitrones, Inorganica Chimica Acta, 380 (2012) 78-89.
[5] A.S. Novikov, M.L. Kuznetsov, A.J.L. Pombeiro, Theory of the formation and decomposition of n-heterocyclic aminooxycarbenes through metal-assisted [2+3]-dipolar cycloaddition/retro-cycloaddition, Chemistry - A European Journal, 19 (2013) 2874-2888.

[6] A.S. Novikov, M.L. Kuznetsov, A.J.L. Pombeiro, N.A. Bokach, G.B. Shul'pin, Generation of HO• radical from hydrogen peroxide catalyzed by aqua complexes of the Group III metals $[M(H_2O)_n]^{3+}$ (M = Ga, In, Sc, Y, or La): A Theoretical Study, ACS Catalysis, 33, (2013) 1195-1208.
[7] A.A. Melekhova, A.S. Novikov, K.V. Luzyanin, N.A. Bokach, G.L. Starova, V.V. Gurzhiy, V.Y. Kukushkin, Tris-isocyanide copper(I) complexes: Synthetic, structural, and theoretical study, Inorganica Chimica Acta, 434 (2015) 31-36.
[8] A.S. Novikov, 1,3-Dipolar cycloaddition of nitrones to transition metal-bound isocyanides: DFT and HSAB principle theoretical model together with analysis of vibrational spectra, Journal of Organometallic Chemistry, 797 (2015) 8-12.
[9] K.I. Kulish, A.S. Novikov, P.M. Tolstoy, D.S. Bolotin, N.A. Bokach, A.A. Zolotarev, V.Y. Kukushkin, Solid state and dynamic solution structures of O-carbamidine amidoximes gives further insight into the mechanism of zinc(II)-mediated generation of 1,2,4-oxadiazoles, Journal of Molecular Structure, 1111 (2016) 142-150.
[10] A.S. Novikov, M.L. Kuznetsov, B.G.M. Rocha, A.J.L. Pombeiro, G.B. Shul'pin, Oxidation of olefins with H_2O_2 catalysed by salts of group III metals (Ga, In, Sc, Y and La): epoxidation versus hydroperoxidation, Catalysis Science & Technology, 6 (2016) 1343-1356.
[11] F. Li, H. Asadi, DFT study of the effect of platinum on the H_2 gas sensing performance of ZnO nanotube: explaining the experimental observations, Journal of Molecular Liquids, (2020) 113139.
[12] M.D. Mohammadi, H.Y. Abdullah, The adsorption of chlorofluoromethane on pristine, and Al-and Ga-doped boron nitride nanosheets: a DFT, NBO, and QTAIM study, Journal of Molecular Modeling, 26 (2020) 1-15.
[13] M.D. Mohammadi, H.Y. Abdullah, Theoretical study of the adsorption of amantadine on pristine, Al-, Ga-, P-, and As-doped boron nitride nanosheets: a PBC-DFT, NBO, and QTAIM study, Theoretical Chemistry Accounts, 139 (2020) 1-17.
[14] M.D. Mohammadi, H.Y. Abdullah, The adsorption of bromochlorodifluoromethane on pristine and Ge-doped silicon carbide nanotube: a PBC-DFT, NBO, and QTAIM study, Structural Chemistry, (2020) 1-14.
[15] M.D. Mohammadi, I.H. Salih, H.Y. Abdullah, An Ultimate Investigation on the adsorption of amantadine on pristine and decorated fullerenes C59X (X= Si, Ge, B, Al, Ga, N, P, and As): A DFT, NBO, and QTAIM Study, Journal of Theoretical and Computational Chemistry, (2020).
[16] E. Nemati-Kande, M. Abbasi, M. Doust Mohammadi, DFT, QTAIM and NBO investigation of the interaction of rare gases with pristine and decorated boron nitride nanotube, ChemistrySelect, 3 (2018) 9833-9840.
[17] E. Nemati-Kande, M. Abbasi, M.D. Mohammadi, DFT studies on the interactions of pristine, Al and Ga-doped boron nitride nanosheets with CH_3X (X= F, Cl and Br), Journal of Molecular Structure, 1199 (2020) 126962.
[18] E. Nemati-Kande, M. Abbasi, M.D. Mohammadi, Feasibility of Pristine and Decorated AlN and SiC Nanotubes in Sensing of Noble Gases: A DFT study, ChemistrySelect, 4 (2019) 2453-2462.
[19] H.W. Kroto, J.R. Heath, S.C. O'Brien, R.F. Curl, R.E. Smalley, C60: Buckminsterfullerene, Nature, 318 (1985) 162-163.
[20] H.-S. Wu, F.-Q. Zhang, X.-H. Xu, C.-J. Zhang, H. Jiao, Geometric and energetic aspects of aluminum nitride cages, The Journal of Physical Chemistry A, 107 (2003) 204-209.
[21] J. Beheshtian, Z. Bagheri, M. Kamfiroozi, A. Ahmadi, A comparative study on the $B_{12}N_{12}$, $Al_{12}N_{12}$, $B_{12}P_{12}$ and $Al_{12}P_{12}$ fullerene-like cages, Journal of Molecular Modeling, 18 (2012) 2653-2658.
[22] T. Oku, A. Nishiwaki, I. Narita, Formation and atomic structure of $B_{12}N_{12}$ nanocage clusters studied by mass spectrometry and cluster calculation, Science and Technology of Advanced Materials, 5 (2004) 635.
[23] X. Michalet, F.F. Pinaud, L.A. Bentolila, J.M. Tsay, S. Doose, J. J. Li, G. Sundaresan, A. Wu, S. Gambhir, S. Weiss, Quantum dots for live cells, in vivo imaging, and diagnostics, Science, 307 (2005) 538-544.

[24] C. Yen, M. Mahmoud, M. El-Sayed, Photocatalysis in gold nanocage nanoreactors, The Journal of Physical Chemistry A, 113 (2009) 4340-4345.
[25] K. Matsuura, N. Kimizuka, T. Yamashita, DNA nanocage by self-organization of DNA and process for producing the same, and DNA nanotube and molecule carrier using the same, Google Patents, 2008.
[26] F. Meng, B. Sana, Y. Li, Y. Liu, S. Lim, X. Chen, Bioengineered tunable memristor based on protein nanocage, Small, 10 (2014) 277-283.
[27] H. Tavakol, D. Shahabi, DFT, QTAIM, and NBO study of adsorption of rare gases into and on the surface of sulfur-doped, single-wall carbon nanotubes, The Journal of Physical Chemistry C, 119 (2015) 6502-6510.
[28] E. Vessally, E. Ahmadi, M.D. Esrafili, A. Hosseinian, Adsorption and decomposition of formaldehyde on the $B_{12}N_{12}$ nanostructure: a density functional theory study, Monatshefte für Chemie-Chemical Monthly, 148 (2017) 1727-1731.
[29] A.A. Peyghan, H. Soleymanabadi, Computational study on ammonia adsorption on the $X_{12}Y_{12}$ nano-clusters (X= B, Al and Y= N, P), Current Science, (2015) 1910-1914.
[30] J. Beheshtian, Z. Bagheri, M. Kamfiroozi, A. Ahmadi, Toxic CO detection by $B_{12}N_{12}$ nanocluster, Microelectronics Journal, 42 (2011) 1400-1403.
[31] D. Quiñonero, A. Frontera, P.M. Deya, Feasibility of single-walled carbon nanotubes as materials for CO_2 adsorption: a DFT study, The Journal of Physical Chemistry C, 116 (2012) 21083-21092.
[32] M.T. Baei, Si-Doped $B_{12}N_{12}$ Nanocage as an Adsorbent for Dissociation of N_2O to N_2 Molecule, Heteroatom Chemistry, 24 (2013) 476-481.
[33] H. Cui, Y. Yong, H. Jiang, L. Yang, S. Wang, G. Zhang, M. Guo, X. Li, The $M_{12}N_{12}$ (M= Al, Ga) clusters as potential sensors for NO, NO_2 and HCN detection, Materials Research Express, 4 (2017) 015009.
[34] V. Tozzini, F. Buda, A. Fasolino, Spontaneous formation and stability of small GaP fullerenes, Physical Review Letters, 85 (2000) 4554.
[35] A. Ektarawong, S.I. Simak, B. Alling, First-principles prediction of stabilities and instabilities of compounds and alloys in the ternary B-As-P system, Physical Review B, 96 (2017) 024202.
[36] L. Guo, Evolution of the electronic structure and properties of neutral and charged aluminum arsenide clusters: A comprehensive analysis, Computational Materials Science, 42 (2008) 489-496.
[37] J. Wang, L. Ma, J. Zhao, G. Wang, X. Chen, R. Bruce King, Electronic and magnetic properties of manganese and iron-doped Ga n As n nanocages (n= 7–12), The Journal of Chemical Physics, 129 (2008) 044908.
[38] M. Omidi, H.R. Shamlouei, M. Noormohammadbeigi, The influence of Sc doping on structural, electronic and optical properties of $Be_{12}O_{12}$, $Mg_{12}O_{12}$ and $Ca_{12}O_{12}$ nanocages: a DFT study, Journal of Molecular Modeling, 23 (2017) 82.
[39] H. Jouypazadeh, H. Farrokhpour, DFT and TD-DFT study of the adsorption and detection of sulfur mustard chemical warfare agent by the C_{24}, $C_{12}Si_{12}$, $Al_{12}N_{12}$, $Al_{12}P_{12}$, $Be_{12}O_{12}$, $B_{12}N_{12}$ and $Mg_{12}O_{12}$ nanocages, Journal of Molecular Structure, 1164 (2018) 227-238.
[40] M. Solimannejad, S. Kamalinahad, E. Shakerzadeh, Silicon carbide nanotubes (SiCNTs) serving for catalytic decomposition of toxic diazomethane (DAZM) gas: a DFT study, Molecular Physics, 116 (2018) 414-422.
[41] W. Kohn, L.J. Sham, Self-consistent equations including exchange and correlation effects, Physical Review, 140 (1965) A1133.
[42] P. Hohenberg, W. Kohn, Inhomogeneous electron gas, Physical Review, 136 (1964) B864.
[43] T. Yanai, D.P. Tew, N.C. Handy, A new hybrid exchange-correlation functional using the Coulomb-attenuating method (CAM-B3LYP), Chemical Physics Letters, 393 (2004) 51-57.
[44] Y. Zhao, D.G. Truhlar, The M06 suite of density functionals for main group thermochemistry, thermochemical kinetics, noncovalent interactions, excited states, and transition elements: two new functionals and systematic testing of four M06-class functionals and 12 other functionals, Theoretical Chemistry Accounts, 120 (2008) 215-241.
[45] J.-D. Chai, M. Head-Gordon, Long-range corrected hybrid density functionals with damped atom-atom dispersion corrections, Physical Chemistry Chemical Physics, 10 (2008) 6615-6620.

[46] S. Grimme, J. Antony, S. Ehrlich, H. Krieg, A consistent and accurate ab initio parametrization of density functional dispersion correction (DFT-D) for the 94 elements H-Pu, The Journal of Chemical Physics, 132 (2010) 154104.
[47] T.V. Russo, R.L. Martin, P.J. Hay, Density functional calculations on first-row transition metals, The Journal of Chemical Physics, 101 (1994) 7729-7737.
[48] R. Dennington, T.A. Keith, J.M. Millam, GaussView, version 6.0. 16, Semichem Inc. Shawnee Mission KS, (2016).
[49] J. Baker, An algorithm for geometry optimization without analytical gradients, Journal of Computational Chemistry, 8 (1987) 563-574.
[50] M.J. Frisch, G.W. Trucks, H.B. Schlegel, G.E. Scuseria, M.A. Robb, J.R. Cheeseman, G. Scalmani, V. Barone, G.A. Petersson, H. Nakatsuji, X. Li, M. Caricato, A.V. Marenich, J. Bloino, B.G. Janesko, R. Gomperts, B. Mennucci, H.P. Hratchian, J.V. Ortiz, A.F. Izmaylov, J.L. Sonnenberg, Williams, F. Ding, F. Lipparini, F. Egidi, J. Goings, B. Peng, A. Petrone, T. Henderson, D. Ranasinghe, V.G. Zakrzewski, J. Gao, N. Rega, G. Zheng, W. Liang, M. Hada, M. Ehara, K. Toyota, R. Fukuda, J. Hasegawa, M. Ishida, T. Nakajima, Y. Honda, O. Kitao, H. Nakai, T. Vreven, K. Throssell, J.A. Montgomery Jr., J.E. Peralta, F. Ogliaro, M.J. Bearpark, J.J. Heyd, E.N. Brothers, K.N. Kudin, V.N. Staroverov, T.A. Keith, R. Kobayashi, J. Normand, K. Raghavachari, A.P. Rendell, J.C. Burant, S.S. Iyengar, J. Tomasi, M. Cossi, J.M. Millam, M. Klene, C. Adamo, R. Cammi, J.W. Ochterski, R.L. Martin, K. Morokuma, O. Farkas, J.B. Foresman, D.J. Fox, Gaussian 16 Rev. C.01, Wallingford, CT, 2016.
[51] T. Lu, F. Chen, Multiwfn: A multifunctional wavefunction analyzer, Journal of Computational Chemistry, 33 (2012) 580-592.
[52] N.M. O'boyle, A.L. Tenderholt, K.M. Langner, Cclib: A library for package-independent computational chemistry algorithms, Journal of Computational Chemistry, 29 (2008) 839-845.
[53] S.F. Boys, F. Bernardi, The calculation of small molecular interactions by the differences of separate total energies. Some procedures with reduced errors, Molecular Physics, 19 (1970) 553-566.
[54] J. Foresman, A. Frisch, Exploring Chemistry With Electronic Structure Methods: A Guide to Using Gaussian, Pittsburgh, PA: Gaussian, Inc, 1996.
[55] J.-L. Bredas, Mind the gap!, Materials Horizons, 1 (2014) 17-19.
[56] F. Weinhold, *Discovering chemistry with natural bond orbitals*, John Wiley & Sons, 2012.
[57] R.S. Mulliken, Electronic population analysis on LCAO-MO molecular wave functions. I, The Journal of Chemical Physics, 23 (1955) 1833-1840.
[58] I. Mayer, Improved definition of bond orders for correlated wave functions, Chemical Physics Letters, 544 (2012) 83-86.
[59] O.V. Sizova, L.V. Skripnikov, A.Y. Sokolov, Symmetry decomposition of quantum chemical bond orders, Journal of Molecular Structure: THEOCHEM, 870 (2008) 1-9.
[60] I. Mayer, P. Salvador, Overlap populations, bond orders and valences for 'fuzzy'atoms, Chemical Physics Letters, 383 (2004) 368-375.
[61] T. Lu, F. Chen, Bond order analysis based on the Laplacian of electron density in fuzzy overlap space, The Journal of Physical Chemistry A, 117 (2013) 3100-3108.
[62] C.F. Matta, Hydrogen-Hydrogen Bonding: The Non-Electrostatic Limit of Closed-Shell Interaction Between Two Hydro, Hydrogen Bonding-New Insights, Springer, 2006, pp. 337-375.
[63] H.J. Bohórquez, R.J. Boyd, C.F. Matta, Molecular model with quantum mechanical bonding information, The Journal of Physical Chemistry A, 115 (2011) 12991-12997.
[64] E.R. Johnson, S. Keinan, P. Mori-Sánchez, J. Contreras-García, A.J. Cohen, W. Yang, Revealing noncovalent interactions, Journal of the American Chemical Society, 132 (2010) 6498-6506.
[65] J. Contreras-García, E.R. Johnson, S. Keinan, R. Chaudret, J.-P. Piquemal, D.N. Beratan, W. Yang, NCIPLOT: a program for plotting noncovalent interaction regions, Journal of Chemical Theory and Computation, 7 (2011) 625-632.